Tight-binding coherent potential approximation study of ferromagnetic $La_{2/3}Ba_{1/3}MnO_3$

D. A. Papaconstantopoulos
Complex Systems Theory Branch, Naval Research Laboratory, Washington, DC 20375

W. E. Pickett
Department of Physics, University of California, Davis, California 95616

(Received 19 November 1997)

The local-spin-density band structure of a virtual-crystal model of ferromagnetic $La_{2/3}Ba_{1/3}MnO_3$, reported earlier by Pickett and Singh [Phys. Rev. B **53**, 1146 (1996)], has been fit to an accurate orthogonal tight-binding (TB) model. This TB Hamiltonian has spin-independent hopping parameters, and the exchange splitting is confined solely to the Mn on-site parameters $\varepsilon_{t_{2g}\downarrow}-\varepsilon_{t_{2g}\uparrow}=3.44$ eV and $\varepsilon_{e_g\downarrow}-\varepsilon_{e_g\uparrow}=2.86$ eV. The crystal-field splitting, as reflected in the Mn d energies, is 1.77 eV for majority spin and 1.19 eV for minority spin. Oxygen $p\sigma$ and $p\pi$ states are allowed distinct site energies, and the derived crystal-field splitting is $\varepsilon_{p\pi}-\varepsilon_{p\sigma}=1.47$ eV. Local Mn d site energy disorder, arising from the random distribution of La^{3+} and Ba^{2+} ions, has been treated within the TB coherent potential approximation. The intrinsic resistivity in the fully polarized phase from this charge disorder is estimated to be 15 $\mu\Omega$ cm. [S0163-1829(98)05020-6]

I. INTRODUCTION

The class of manganites $A^{3+}_{1-x}B^{2+}_{x}MnO_3$ with perovskite structure were found by von Helmolt *et al.*,[1] Jin *et al.*,[2] and numerous following investigators to display a negative ''colossal magnetoresistance'' (CMR) at the onset of ferromagnetic order for $x\approx\frac{1}{3}$ as the temperature is lowered. Since that time, a remarkable variety of behaviors has been observed as x, temperature T, magnetic field H, and constituents A and B are varied.[3] In addition to CMR, various charge- and spin-ordered phases are observed. Insulator-to-metal transitions have been observed as a function of temperature (original CMR observations), of field, of cation constituents, of imposed x-ray flux, and (at the proper temperature) of O isotope mass.[4] The system is obviously close to a metal-insulator instability that can be tuned in several ways, with varying outcomes.

Theoretical modeling of these materials has proceeded in several directions. A popular approach has been to pursue the ''double exchange'' idea proposed by Zener[5] and extended in very early work.[6,7] There are conflicting conclusions reported in the literature, even for the simplest models.[8,9] More complex models have been proposed; for example, Mazzaferro, Balsiero, and Alascio[10] introduced a model that included charge disorder, spin disorder, and Coulomb repulsion, but only studied it in certain limiting cases. It is still unclear what aspects of the manganites are essential for the unusual phenomena that have been observed.[3]

The electronic structure of $LaMnO_3$, $CaMnO_3$, and certain intermediate concentrations (ordered supercells and virtual-crystal treatments) have been studied extensively within local-spin-density-functional theory in a variety of ways.[11–16] In Secs. II and III, we report an accurate tight binding (TB) analysis of the Slater-Koster type[17] for the band structure of the $x=\frac{1}{3}$ virtual-crystal alloy in the ferromagnetically aligned state.[16] This analysis allows the identification of the important hopping amplitudes that are needed for model Hamiltonian studies. We also obtain crystal-field splittings and exchange splittings on the Mn ion that are necessary to address the colossal magnetoresistance phenomena that are observed in this system.

To study an aspect that has been neglected so far, the effects on the carriers of charge disorder in the cation (La-Ba) sublattice, in Sec. IV we present a TB coherent potential approximation (CPA) treatment of the ferromagnetic system with randomly distributed cations. This study quantifies the effects of disorder scattering on the carriers, and leads to quantitative estimates of the minimum resistivity achievable at low temperature. The way in which the TB parametrization is done also prepares the methods to treat spin disorder at a later stage.

II. TIGHT-BINDING HAMILTONIAN

The TB fit of the band structure follows the methods and conventions established earlier.[18] In these manganites the O p bands are centered well below the Mn d bands, and the bands around E_F can be readily identified as the Mn d bands. Therefore a minimal basis set might be comprised solely of effective d states on the Mn ions. However, since the direct overlap of the actual d orbitals on nearest-neighbor Mn ions is negligible, the hybridization via the intermediary O p states is an essential feature of the electronic structure. To allow more flexibility in representing the band structure at the top of the d bands, we have also included La (Ba) s and d states (which lie lower than La p states) and Mn s states, as well as the Mn d and O p states.

As is conventional for accurate fits, the crystal-field splitting of d states at a cubic site is taken into account ($\varepsilon_{e_g}\neq\varepsilon_{t_{2g}}$) on both Mn and La ions. In addition, an unconventional but very useful feature is to allow the crystal-field splitting of the O p states. The O site symmetry is C_4 (tetragonal), leading to a p_σ orbital and two p_π orbitals (taking Mn to lie along the local $\hat{z}$ axis of the O ion). This distinction leads to one additional on-site parameter.

The Hamiltonian is set up assuming orthogonal basis orbitals. Such orbitals correspond to Wannier functions, and the ''Mn *d* orbital,'' for example, will represent in addition to the Mn *d* atomic orbital a combination of neighboring O *p* orbitals with the same symmetry. In our fit, 20 bands in each spin channel have been used, with 35 evenly spaced *k* points in the irreducible Brillouin zone for each band. For the high-symmetry *k* points Γ and *R* we carried out the block diagonalization of our 21×21 secular equation and fitted the 21st band as well. This was fairly important in improving the TB fit by identifying the correct symmetry of the states. Only first-neighbor interactions have been included, with the exception that second-neighbor O-O parameters were retained. The rms deviation between corresponding linear augmented plane-wave and TB eigenvalues was 0.20 eV for the majority spin and 0.15 eV for the minority spin over the entire 20 bands. For the five *d* bands that are of greatest interest, the rms errors are 0.12 eV for the majority bands and 0.08 eV for the minority bands.

One way of proceeding is to fit majority and minority bands completely separately, which was done initially. However, in what we present here we have followed a more physical route by fitting both directions of spin with hopping parameters that are independent of spin. In addition, the on-site parameters are spin split only for the Mn e_g and t_{2g} states; other on-site parameters are spin independent. We find that a very good fit to both spin directions can be obtained with this procedure, and it leads to a more pedagogical interpretation of the results. The total number of parameters, which is 35, is also reduced by almost a factor of 2 from the number ($66=33\times2$) that would have been used for an equivalent basis for the two spins separately.

TABLE I. Values of the 35 tight-binding parameters (in eV, relative to the Fermi level) obtained from least squares fit to the LAPW band structure. The spin splitting is confined to the Mn *d* on-site energies (spin directions denoted by $\uparrow$ and $\downarrow$).

Atom	Parameter	Value (eV)
La	ε_s	10.59
La	$\varepsilon_{t_{2g}}$	4.83
La	ε_{e_g}	4.60
Mn	ε_s	9.90
Mn	$\varepsilon_{t_{2g}\uparrow},\varepsilon_{t_{2g}\downarrow}$	$-2.80,+0.64$
Mn	$\varepsilon_{e_g\uparrow},\varepsilon_{e_g\downarrow}$	$-1.03,+1.83$
O	$\varepsilon_{p\sigma}$	-4.04
O	$\varepsilon_{p\pi}$	-2.57
La-La	$ss\sigma$	0.00
La-La	$sd\sigma$	$+0.34$
La-La	$dd\sigma$	-0.85
La-La	$dd\pi$	$+0.17$
La-La	$dd\delta$	-0.02
Mn-Mn	$ss\sigma$	-0.48
Mn-Mn	$sd\sigma$	$+0.19$
Mn-Mn	$dd\sigma$	-0.16
Mn-Mn	$dd\pi$	-0.12
Mn-Mn	$dd\delta$	-0.01
$(\text{O-O})_1$	$pp\sigma$	$+0.46$
$(\text{O-O})_1$	$pp\pi$	-0.07
$(\text{O-O})_2$	$pp\sigma$	$+0.06$
$(\text{O-O})_2$	$pp\pi$	-0.04
La-Mn	$ss\sigma$	-0.43
La-Mn	$sd\sigma$	$+0.32$
La-Mn	$dd\sigma$	$+0.28$
La-Mn	$dd\pi$	-0.02
La-Mn	$dd\delta$	0.09
La-Mn	$ds\sigma$	-0.09
La-O	$dp\sigma$	-1.76
La-O	$dp\pi$	0.53
Mn-O	$sp\sigma$	-1.17
Mn-O	$dp\sigma$	1.81
Mn-O	$dp\pi$	-0.89

III. FIT TO THE VIRTUAL-CRYSTAL ALLOY

A. Examination of parameters

The TB parameters are presented in Table I. It should be kept in mind that the parameters of this orthogonal TB representation may not represent atomic values accurately; however, most model Hamiltonian approaches desire parameters in an orthogonal (Wannier) representation. In a TB fit, it is common to focus on the ''minimal basis set,'' which in this case comprises the Mn *d* and the O *p* states, and to either neglect or at least downplay other states and the associated parameters.

On-site energies. The La *s* and *d* and Mn *s* site energies lie 5–10 eV above the Fermi level, and will not be discussed in detail. The Mn crystal-field splitting $\varepsilon_{e_g}-\varepsilon_{t_{2g}}$ is spin-dependent: 1.77 eV for the majority spin where the t_{2g} states are completely occupied and often treated as ''corelike,''[8,9] and 1.19 eV for the minority spin where Mn *d* occupation is slight. Somewhat surprising is the large crystal-field splitting on the O ion, $\varepsilon_{p\pi}-\varepsilon_{p\sigma}=1.47$ eV, justifying our decision to allow this splitting. The resulting exchange splittings on the Mn *d* states are 3.44 eV for t_{2g} and 2.86 eV for e_g. Note that these values are distinct from what would be obtained from Γ_{12} and $\Gamma_{25'}$ eigenvalues, which contain strong contributions from hybridization processes.

The other energy difference of interest is the mean difference between Mn *d* and O *p* levels,

$$\varepsilon_d-\varepsilon_p\equiv\left(\tfrac{3}{5}\overline{\varepsilon}_{t_{2g}}+\tfrac{2}{5}\overline{\varepsilon}_{e_g}\right)-\left(\tfrac{1}{3}\varepsilon_{p\sigma}+\tfrac{2}{3}\varepsilon_{p\pi}\right)$$

$$=-0.47-(-3.07)=2.60\ \text{eV}. \qquad (1)$$

Here $\overline{\varepsilon}$ indicates the spin-averaged value. This value of $\varepsilon_d-\varepsilon_p$ is smaller that would be estimated from looking at the density of states, which includes the effect of band mixing that leads to net repulsion between the Mn *d* and the O *p* bands.

Transfer integrals. The Mn-O hopping processes are expected to be the most important, and we obtain the rather large values of $(dp\sigma)=+1.81$ eV and $(dp\pi)=-0.89$ eV. The direct nearest-neighbor O-O hopping parameter $(pp\sigma)=0.46$ is also important, while $(pp\pi)=-0.07$ is substantially smaller. Second-neighbor *p*-*p* hopping is unimportant. The signature of Wannier (orthogonal) orbitals shows up in the Mn *d*-*d* parameters. Whereas direct hopping between *atomic* orbitals should be negligible due to the dis-

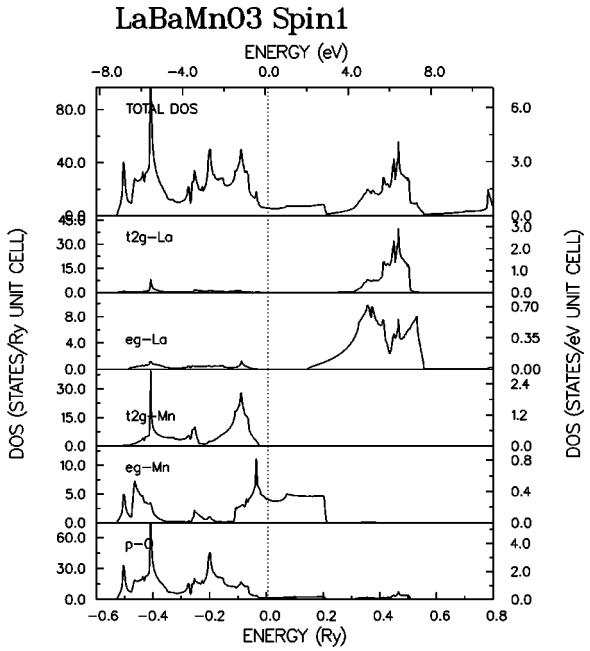

FIG. 1. Total and atom-decomposed densities of majority states resulting from the tight-binding fit described in the text. The energy scale extends throughout the range of bands that were fit.

tance, the parameters $(dd\sigma)=-0.16$ eV and $(dd\pi)=-0.12$ eV are not negligible. Several hopping parameters involving La s and d and Mn s are large, indicating that these states are active in providing the good fit.

B. Comparison to LAPW bands

The densities of states (DOS) obtained from the TB fit, shown in Figs. 1 and 2 for majority and minority spins, respectively, are very similar to the first-principles

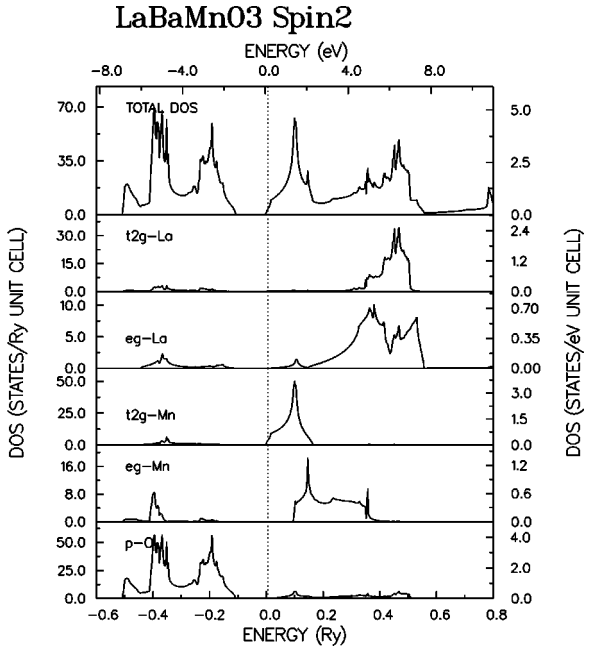

FIG. 2. Total and atom-decomposed densities of minority states resulting from the tight-binding fit described in the text, plotted as in Fig. 1. Note the slightly occupied pocket at the Fermi level.

calculation[20] especially near the Fermi level. The majority t_{2g} states are fully occupied, and the e_g are half-filled, providing a large density of states for conduction. The minority t_{2g} states are only slightly occupied, meaning the Mn ion is in its Hund's-rule high-spin configuration. The bands and DOS near E_F are most important, and they are crucial in the minority channel where E_F lies near a band edge. The distinction between t_{2g} and e_g DOS was not plotted in Ref. 20. Figure 1 illustrates that the strong $dp\sigma$ bonding drags Mn e_g character into the lower p bands, and leads to O $p\sigma$ character in the broadband crossing the Fermi level.

IV. COHERENT POTENTIAL APPROXIMATION

The Korringa-Kohn-Rostoker CPA calculation of Butler, Zhang, and MacLaren (BZM) (Ref. 21) treated disorder on the cation (La/Ba) site only, replacing this site as usual with the ''average scatterer'' determined self-consistently. The carriers experience disorder only to the extent that their wave function has amplitude on the cation site. We take the viewpoint that the carriers, being primarily of Mn d character with some O p character but negligible amplitude on the cation site, will ''feel'' the disorder primarily through a shift of the Mn d site energy arising from the distribution of local cation charges (La^{3+}, Ba^{2+}) on first- and second-neighbor shells. The lowest La and Ba states (d) are completely unoccupied, as can be seen in Figs. 1 and 2, so we neglect cation d-state disorder. In a sense then our treatment is complementary to that of BZM, who evaluated the effect of disorder on the cation site but neglected the induced disorder on the Mn site.

A. Specification of disorder

The determination of the d-site energy for different local environments was obtained previously by Pickett and Singh[16] from calculations of ordered (La,Ba)MnO_3 supercells. Both the associated e_g band edge and core-level energies reflected the change in on-site energy due to the local change in configuration of La^{3+} and Ba^{2+} ions. The distribution of these site energies for more general cation arrangements is modeled as random La^{3+} and Ba^{2+} charges screened by a local dielectric constant $\epsilon=10$, which reproduced the supercell results. A Mn ion can have nine distinct site energies due to the occupation of the first-neighbor shell (eight La; seven La + one Ba; six La + two Ba; etc.), and each of these is split further by the seven distinct energy shifts from the second-neighbor shell. Our TB-CPA treatment then becomes a multicomponent CPA with 63 different types of Mn ions, differing only by their site energy.

In Table II we list the possible configurations, the resulting energy shift, and the relative probability of occurrence, for both first- and second-neighbor shells. The distribution of Mn site energies was shown graphically in Ref. 16. The full width at half maximum of the (slightly broadened) distribution about the mean is 0.5 eV, which is the first measure of disorder broadening in this system.[20]

One may consider whether the local configuration of ions around a Mn site is of importance. For example, two Ba ions in the first shell may be adjacent to each other (on one side of the Mn site) or, at the other extreme, they might lie on op-

TABLE II. The list of all configurations of the first- and second-neighbor shells, if populated randomly by La^{3+} and Ba^{2+} ions with the average occupation constrained to be $x=\frac{1}{3}$. The energy shift $\delta\varepsilon_d$ (eV) is given with respect to the mean Mn d site energy. The multiplicity is the number of ways the set of atoms can be distributed on the shell, and the relative probability reflects the fact that La^{3+} occupation of any site is twice as likely as Ba^{2+} occupation. The product gives the relative likelihood for that configuration occuring in the $x=\frac{1}{3}$ crystal.

La^{3+},Ba^{2+}	Mult.	Rel. Prob.	Product	$\delta\varepsilon_d$
		First Shell		
8 0	1	256	256	$-\frac{8}{24}$
7 1	8	128	1024	$-\frac{5}{24}$
6 2	28	64	1792	$-\frac{2}{24}$
5 3	56	32	1792	$+\frac{1}{24}$
4 4	70	16	1120	$+\frac{4}{24}$
3 5	56	8	448	$+\frac{7}{24}$
2 6	28	4	112	$+\frac{10}{24}$
1 7	8	2	16	$+\frac{13}{24}$
0 8	1	1	1	$+\frac{16}{24}$
		Second Shell		
6 0	1	64	64	$-\frac{2}{9}$
5 1	6	32	192	$-\frac{1}{9}$
4 2	15	16	240	$+\frac{0}{9}$
3 3	20	8	160	$+\frac{1}{9}$
2 4	15	4	60	$+\frac{2}{9}$
1 5	6	2	12	$+\frac{3}{9}$
0 6	1	1	1	$+\frac{4}{9}$

posite sides of the Mn ion. Within a single-site theory such as the CPA, differences that would arise cannot be treated, except to the extent that the t_{2g} orbitals are affected differently from the e_g ions (whose site energies we keep distinct). The first such correction is dipolar, with a vanishing shift of the site energy of d orbitals. Quadrupolar terms may shift e_g orbitals with respect to t_{2g} orbitals, but we expect such corrections to be much smaller than those we have kept in the CPA calculation.

B. CPA formalism

In the formalism that we follow,[22] only diagonal disorder is treated. The CPA condition of zero average scattering in our case involves a sum with 63 terms,

$$\sum_{1=1}^{63} c_i \hat{t}_i = 0, \tag{2}$$

where the probabilities c_i can be found from the values in the product column in Table II, with sum normalized to unity. The scattering matrices $\hat{t}_i$ have the form[22]

$$\hat{t}_i = (\hat{\varepsilon}_i - \hat{\Sigma})\{1 - (\hat{\varepsilon}_i - \hat{\Sigma})\hat{G}\}^{-1}, \tag{3}$$

where $\hat{\varepsilon}_i$ is a diagonal matrix containing the on-site TB energies for the Mn d levels ($\varepsilon_{t_{2g}}$ and ε_{e_g} in Table I) modified for each of the 63 configurations by adding the corresponding quantity $\delta\varepsilon_d$ from Table II. $\hat{\Sigma}$ is also a 5×5 diagonal matrix containing two distinct self-energies $\hat{\Sigma}_{t_{2g}}$ and $\hat{\Sigma}_{e_g}$.

$\hat{G}$ is the Green's function given by an integral over the Brillouin zone (BZ):

$$\hat{G}(z,\Sigma) = \frac{\Omega_c}{(2\pi)^3}\int_{BZ} \frac{d^3k}{z - \hat{H}(k,\Sigma)}, \tag{4}$$

where z is the complex energy and Ω_c is the unit cell volume. In this equation, $\hat{H}(k,\Sigma)$ is the full 21×21 TB Hamiltonian modified by replacing the Mn d energies $\varepsilon_{t_{2g}}$ and ε_{e_g} by $\Sigma_{t_{2g}}$ and Σ_{e_g}, respectively. Equations (1)–(3) are solved self-consistently by a Newton-Raphson method, with a uniform grid of 969 k points in the irreducible BZ and an imaginary part of the energy of 8 mRy, to determine Σ and $\hat{G}$ at each energy. Note that this procedure is repeated separately for the majority and minority spins, which means that we treat the disorder corresponding to the 63 different ''Mn sites,'' but do not treat spin flips on a Mn site.

Having calculated $\hat{G}$ we obtain the angular momentum decomposed densities of states, for each spin and angular momentum ℓ separately, from the expression

$$N_\ell(\varepsilon) = -\frac{1}{\pi}\lim_{z\to\varepsilon^+} \mathrm{Im}\, \hat{G}_{\ell\ell}(z,\Sigma). \tag{5}$$

The spectral density is given by

$$A(k,\varepsilon) = -\frac{1}{\pi}\sum_{\ell} \mathrm{Im}\, G_{\ell\ell}(k,\varepsilon). \tag{6}$$

$A(k,\varepsilon)$ is the generalization of the band dispersion relation E_k, which in the limit of a periodic crystal becomes $\delta(\varepsilon - E_k)$. Below we will discuss the self-energy relative to the site energy, $\delta\Sigma_i = \Sigma_i - \varepsilon_i$, whose real part gives the energy shift, and whose imaginary part gives the magnitude of the disorder broadening which can be interpreted as an inverse lifetime.

V. DISCUSSION AND COMPARISON WITH EXPERIMENT

Self-energies

In Figs. 3 and 4, the self-energies $\Sigma_i(\varepsilon)$ ($i=e_g,t_{2g}$) are shown for majority and minority spins, respectively. These figures are for solution of the CPA equations with an imaginary part of the energy in Eq. (4) set to 8 mRy. Equivalent results were obtained when a 4 mRy imaginary energy was used. Note that $|\mathrm{Im}\Sigma_i(\varepsilon)|$ is appreciable only where the Mn i DOS is nonzero, and the shape bears some resemblance to the corresponding DOS, broadened somewhat. $\mathrm{Re}\Sigma_i(\varepsilon)$ follows the expected Hilbert transform of $\mathrm{Im}\Sigma_i$.

For the majority spin, $|\mathrm{Im}\Sigma_{t_{2g}}(\varepsilon_F)|$ vanishes, and $|\mathrm{Im}\Sigma_{e_g}(\varepsilon_F)| = 8$ meV. There is a relative energy shift of e_g and t_{2g} states by

$$\mathrm{Re}[\Sigma_{t_{2g}}(\varepsilon_F) - \Sigma_{e_g}(\varepsilon_F)] = 10 \text{ meV}, \tag{7}$$

but since the e_g bands are broad and the t_{2g} bands do not lie at ε_F, this is of no consequence. The important result is the

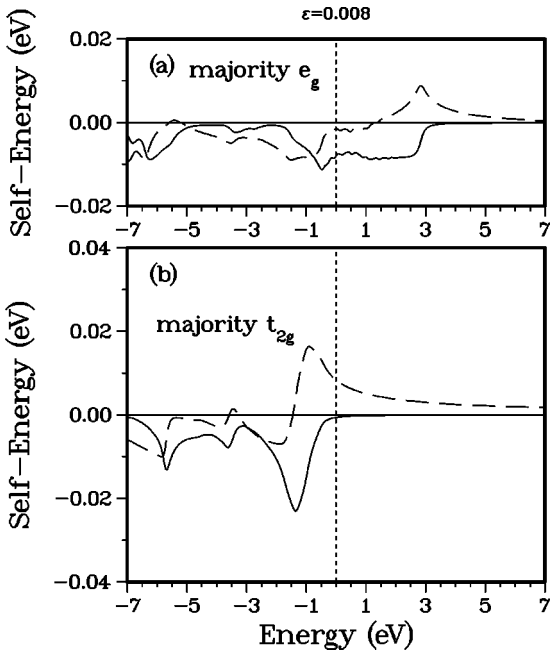

FIG. 3. Real (dashed) and imaginary (solid) parts of the CPA self-energy of the majority-spin states; the quantities plotted are $\Sigma_{e_g}-\varepsilon_{e_g}$ and $\Sigma_{t_{2g}}-\varepsilon_{t_{2g}}$. The scale is with respect to the energies of the tight-binding bands, with Fermi level taken as the zero of energy. The imaginary part of the energy was 8 mRy for this CPA calculation.

broadening, which provides an intrinsic lifetime for the majority carriers of e_g symmetry on the cube and sphere Fermi surfaces:[16,20] $\hbar/\tau=|\mathrm{Im}\Sigma_{e_g}(\varepsilon_F)|=8$ meV. Given the velocity of the carriers,[16] $v_F = (7.1\text{–}7.6)\times10^7$ cm/s, this gives an intrinsic mean free path $\ell=v_F\tau=600$ Å. Using $\rho_0 = 4\pi/\Omega_p^2\tau$, with[16] $\hbar\Omega_p=1.9$ eV, this limiting of transport translates into a minimum residual resistivity $\rho_0=15$ $\mu\Omega$ cm. A value as low as 35 $\mu\Omega$ cm was already reported by Hwang *et al.*[23]

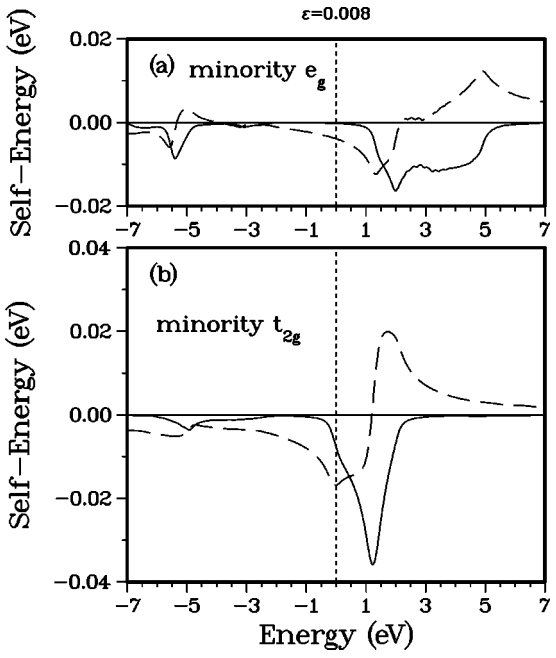

FIG. 4. Real (dashed) and imaginary (solid) parts of the CPA self-energy of the minority-spin states, plotted as in Fig. 4.

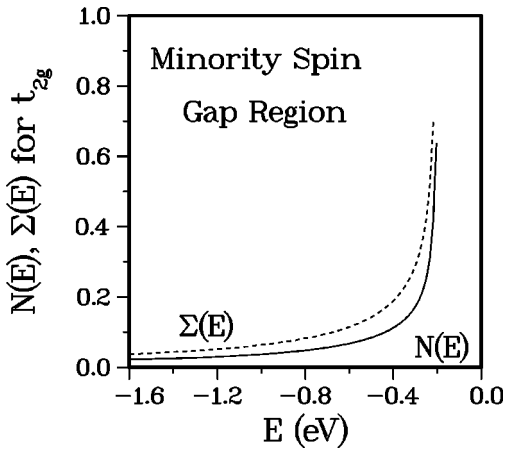

FIG. 5. The minority t_{2g} components of both $N(E)$ (in units of 0.1 states/eV) and the absolute value of $\mathrm{Im}\Sigma(\mathrm{E})$ (meV), illustrating their great similarity in the gap region.

The minority spin is more interesting: if the occupied states are localized, as inferred previously,[16] the ferromagnetic $x=\frac{1}{3}$ material is half-metallic. Only states of t_{2g} character reside at ε_F, so the e_g self-energies will not be discussed. At or very near ε_F $\mathrm{Re}\Sigma_{t_{2g}}(\varepsilon_F)=-18$ meV and $|\mathrm{Im}\Sigma_{t_{2g}}(\varepsilon_F)|=8\text{–}10$ meV. One interesting feature is the shift in energies of different spins at the Fermi level:

$$\mathrm{Re}\Sigma_{t_{2g}\uparrow}(\varepsilon_F)-\mathrm{Re}\Sigma_{e_g\downarrow}(\varepsilon_F)=-16\ \text{meV}. \tag{8}$$

This will result in a transfer of spin from majority to minority. This effect can be estimated as follows. Near the band edge the virtual-crystal DOS $N(\varepsilon)$ goes as $\varepsilon^{1/2}$ so the number of carriers $\mathcal{N}(\varepsilon)\propto\varepsilon^{3/2}$. The relative change in number of carriers is

$$\frac{\delta\mathcal{N}}{\mathcal{N}}=\frac{d\ \log\mathcal{N}}{d\ \log\varepsilon}\frac{\delta\varepsilon}{\varepsilon_F}=\frac{3}{2}\frac{\delta\varepsilon}{\varepsilon_F}. \tag{9}$$

The 10% increase in (minority) Fermi energy ($\delta\varepsilon=16$ meV, $\varepsilon_F=150$ meV) translates into a 15% increase in minority carriers.

This change in the magnetization can be considered as arising from a disorder-induced ''magnetic field'' (relative shift of spin-up and spin-down bands) and as such it will be proportional to the phase space for spins to flip direction, i.e., $N_\uparrow(\varepsilon_F)N_\downarrow(\varepsilon_F)$. If this change in spin moment were treated self-consistently (as it should be), the response of the exchange potential would oppose the change in spin. The net effect is likely to be negligible.

For the question of localization, a shift in the minority Fermi level may become more relevant. If the shift (self-consistently) increases the number of minority carriers, then the minority Fermi level moves farther from the band edge, with a concomitant decrease in the tendency toward localization of all of the carriers. However, the CPA alone is insufficient to determine localization of states or, equivalently, the position of the mobility edge below which electronic states are nonconducting.

In Fig. 5 we show a detail of the gap region, plotting the

t_{2g} minority components of both $N(E)$ and $\mathrm{Im}\Sigma(E)$. It is evident that at the edge of the gap region and below, they behave very similarly. Since this pseudogap lies in a region of a large majority density of states, it will be difficult to resolve its magnitude and energy dependence in many spectroscopies and in thermodynamic properties. Processes involving spin flips, however, such as the NMR spin-lattice relaxation rate or even the magnetic susceptibility, provide a good probe of these minority characteristics. Experimental study, and further theoretical study beyond the CPA, to learn the density dependence and the temperature scaling (at low $T \ll T_C$) will be required for further understanding of the minority-spin pseudogap.

VI. SUMMARY

We have presented a TB parametrization of the band structure of virtual-crystal $La_{2/3}Ba_{1/3}MnO_3$ that is high quality throughout the entire valence-band–conduction-band region, and is particularly accurate in the region of the Fermi level. This parametrization allowed us to extract the exchange splitting of the Mn d states, which are crystal field dependent, and their crystal-field splittings, which are different for different spins. Band effects are dominated by the Mn-O $(dd\sigma)$ and $(dd\pi)$ parameters, as expected, and nearest-neighbor O-O $(pp\sigma)$ hopping is also important. The parametrization has been formulated in a way (hopping processes are spin independent) that makes the treatment of spin disorder straightforward.[19]

Within the CPA, we have calculated the effect on the carriers of the distribution of Mn site energies arising from the random occupation of nearest- and next-nearest-neighbor shells by La^{3+} and Ba^{2+} ions. This model leads to a distribution of 63 different site energies, whose cooperative effect was evaluated within the coherent potential approximation. Due to the averaging that occurs within the CPA, the carrier self-energies (both the energy shift and the broadening) are one order of magnitude smaller than the rms Mn site energy variation. This amount of disorder predicts a minimum resistivity in the low-temperature, saturated ferromagnetic phase of 15 $\mu\Omega$ cm, which is only a factor of 2 less than the lowest reported resistivity we are aware of. For increasing T, magnetic fluctuations increase and become precipitous as long-range magnetic order vanishes at T_C. The TB model introduced in this paper should be useful in studying this dynamic behavior.

ACKNOWLEDGMENTS

We have benefited from technical discussions with D. J. Singh. This work was supported by the U.S. Office of Naval Research.

[1] R. von Helmolt, J. Wecker, B. Holzapfel, L. Schultz, and K. Samwer, Phys. Rev. Lett. **71**, 2331 (1993).
[2] S. Jin, H. M. O'Bryan, T. H. Tiefel, M. McCormack, R. A. Fastnacht, R. Ramesh, and L. H. Chen, Science **264**, 413 (1994).
[3] A good source of references is available in the collection in Physica B **327/328** (1997).
[4] See, for example, Y. Tomioka, A. Asamitsu, H. Kuwahara, and Y. Tokura, J. Phys. Soc. Jpn. **66**, 302 (1997); C. H. Chen and S.-W. Cheong, Phys. Rev. Lett. **76**, 4042 (1996); G.-M. Zhao, M. B. Hunt, H. Keller, and K. A. Müller, Nature (London) **385**, 236 (1997).
[5] C. Zener, Phys. Rev. **82**, 403 (1951).
[6] P. G. de Gennes, Phys. Rev. **118**, 141 (1960).
[7] P. W. Anderson and H. Hasagawa, Phys. Rev. **100**, 675 (1955).
[8] N. Furakawa, J. Phys. Soc. Jpn. **63**, 3414 (1994); **65**, 2734 (1995); **65**, 2754 (1995); **65**, 3164 (1995).
[9] A. J. Millis, P. B. Littlewood, and B. I. Shraiman, Phys. Rev. Lett. **74**, 5144 (1995).
[10] J. Mazzaferro, C. A. Balsiero, and B. Alascio, J. Phys. Chem. Solids **46**, 1339 (1985).
[11] W. E. Pickett and D. J. Singh, Phys. Rev. B **53**, 1146 (1996).
[12] D. D. Sarma, N. Shanthi, S. R. Barman, N. Hamada, H. Sawada, and K. Terakura, Phys. Rev. Lett. **75**, 1126 (1995).
[13] I. Solovyev, N. Hamada, and K. Terakura, Phys. Rev. Lett. **76**, 4825 (1996).
[14] S. Satpathy, Z. S. Popovic, and F. R. Vukajlovic, Phys. Rev. Lett. **76**, 960 (1996).
[15] N. Hamada, H. Sawada, and K. Terakura, in *Spectroscopy of Mott Insulators and Correlated Metals*, edited by A. Fujimori and Y. Tokura (Springer-Verlag, Berlin, 1995), pp. 95–105.
[16] W. E. Pickett and D. J. Singh, Phys. Rev. B **55**, R8642 (1997).
[17] J. C. Slater and G. F. Koster, Phys. Rev. **94**, 1498 (1954).
[18] D. A. Papaconstantopoulos, *Handbook of the Band Structure of Elementary Solids* (Plenum, New York, 1986).
[19] W. E. Pickett, *Proceedings of the Pacific Conference on Condensed Matter Theory: Complex Materials and Strongly Correlated Systems, Seoul, Korea, 1995* [J. Korean Phys. Soc. (Suppl.) **29**, S70 (1996)].
[20] W. E. Pickett and D. J. Singh, J. Magn. Magn. Mater. **172**, 237 (1997).
[21] W. H. Butler, X.-G. Zhang, and J.M. MacLaren, in *Magnetic Ultrathin Films and Multilayers and Surfaces*, edited by E.E. Marinero *et al.*, MRS Symposia Proceedings No. 384 (Materials Research Society, Pittsburgh, 1995), pp. 439–443.
[22] P. M. Laufer and D. A. Papaconstantopoulos, Phys. Rev. B **35**, 9019 (1987).
[23] H. Y. Hwang *et al.*, Phys. Rev. Lett. **77**, 2041 (1996).